JOURNAL OF EXPERIMENTAL AND THEORETICAL PHYSICS, 2024, Vol. 166, No. 6 (12), pp. 826–836

ORDER, DISORDER, AND PHASE TRANSITION IN CONDENSED MEDIA

FULL MAGNETIZATION PROCESS AND MAGNETIC PHASE DIAGRAM OF RARE-EARTH FERRIMAGNETS $R_2Fe_{14}B$

© 2024 N. V. Kostyuchenko[a,b]*, D. I. Plokhov[a,c,d]**, I. S. Tereshina[a,e], G. A. Politova[f,g], Yu. B. Kudasov[h,i], V. V. Platonov[h,i], O. M. Surdin[h,i], D. A. Maslov[h,i], I. S. Strelkov[h], R. V. Kozabaranov[h,i], P. Yu. Katenkov[h,i], A. S. Korshunov[h], I. V. Makarov[h], A. I. Bykov[h], A. V. Filippov[h], E. A. Bychkova[h], P. B. Repin[h], V. D. Selemir[h], A. A. Gorbachevich[a], A. K. Zvezdin[a,c]

[a] *Lebedev Physical Institute of the Russian Academy of Sciences, Moscow, 119991 Russia*

[b] *Moscow Institute of Physics and Technology, Dolgoprudny, Moscow Region, 141701 Russia*

[c] *Prokhorov General Physics Institute of the Russian Academy of Sciences, Moscow, 119991 Russia*

[d] *Patrice Lumumba Peoples' Friendship University of Russia, Moscow, 117198 Russia*

[e] *Physics Faculty of Lomonosov Moscow State University, Moscow, 119991 Russia*

[f] *Baikov Institute of Metallurgy and Materials Science of the Russian Academy of Sciences, Moscow, 119334 Russia*

[g] *Peter the Great St. Petersburg Polytechnic University, St. Petersburg, 195251 Russia*

[h] *Russian Federal Nuclear Center (RFNC-VNIIEF), Sarov, 607188 Russia*

[i] *Sarov Physics and Technology Institute of National Research Nuclear University MEPhI, Sarov, 607186 Russia*

** e-mail: nvkost@gmail.com*

*** e-mail: dmitry@plokhov.ru*

Received July 10, 2024

Revised August 20, 2024

Accepted August 23, 2024

Abstract. Using the example of intermetallic compound $Ho_2Fe_{14}B$ and its hydride $Ho_2Fe_{14}BH_{1.7}$ the process of full magnetization of rare-earth ferrimagnets of the R-Fe-B system has been studied. It is shown that in an external magnetic field of megagauss range, these compounds undergo induced orientational transitions from ferrimagnetic to ferromagnetic state. Based on experimental data, the values of critical fields for these transitions were determined. Magnetic phase diagrams in "magnetic field – temperature" variables were theoretically obtained, and R–Fe exchange interactions constants were calculated.

DOI: 10.31857/S004445102412e083

1. INTRODUCTION

In the Nobel lecture of Academician V. L. Ginzburg [1], a list of fundamental problems in physics and astrophysics that he considered most important for the 21st century is provided, among which the problem of studying the extreme state of matter in ultra-high magnetic fields is mentioned. Mentioning only briefly the fascinating problem of neutron stars with exceptionally high magnetic fields (magnetars) – see, for example, review [2] and

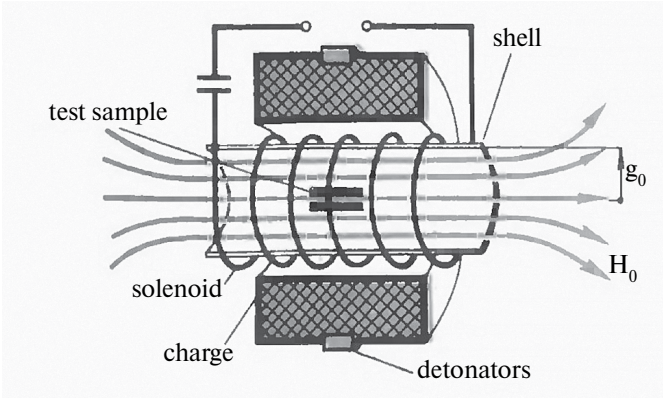

Fig. 1. Schematic diagram of the MC-1 magnetic cumulative generator

recent report [3] about the record-high magnetic field induction of $1.6 \cdot 10^9$ T created by a binary star system – we will focus on studying the properties of magnetic materials in megagauss range fields.

A common method for generating strong and ultra-strong magnetic fields is the magnetic cumulative method, which is based on the ideas of Academician A. D. Sakharov, proposed in the early 1950s [4].

The essence of the method is as follows (Fig. 1): when a capacitor bank discharges into a solenoid-liner, a magnetic flux appears inside it. The detonation of the explosive charge surrounding the liner is synchronized so that under the action of explosion products, it begins to move when the initial magnetic field reaches its maximum. As the liner converges to the center, it compresses the magnetic flux, and since the flux remains approximately constant, the magnetic field induction inside the shell increases. The induction values of magnetic fields generated in this way can reach values exceeding 1000 T [5, 6].

In Russia, the magnetocumulative method of generating high and ultra-high magnetic fields has been successfully developed for many years at RFNC-VNIIEF (Sarov, Nizhny Novgorod region), where a magnetic field pulse was obtained with a record induction of 2800 T [5]. Issues related to the development and application of magnetocumulative generators are detailed in monograph [7], while physical research in ultra-high magnetic fields is covered in review [8].

The magnetocumulative method allows for systematic studies of extreme states of matter, necessary for various fields of physics. In particular, in solid state physics, this method enables direct acquisition of information about crucial microscopic parameters of magnetically ordered materials, primarily exchange constants (intra- and inter-sublattice exchange interactions), crystal field parameters, magnetocrystalline anisotropy constants, etc., based on studying not only magnetic phase transitions but also full magnetization processes, including, for example, the transition of ferrimagnetic materials to a ferromagnetic state induced by an external magnetic field [9, 10], without the need for spectroscopic experiments or complex and labor-intensive theoretical research methods, such as first-principles calculations.

In this work, the magnetization processes of the intermetallic compound $Ho_2Fe_{14}B$ and its hydride $Ho_2Fe_{14}BH_{1.7}$ in magnetic fields of the megagauss range were studied, and magnetic phase diagrams of these compounds were obtained in the variables "magnetic field – temperature". The choice of holmium heavy rare-earth metal for this study is determined by the magnitude of the holmium ion's magnetic moment ($\mu_{\mathrm{Ho}} = 10\mu_B$, where μ_B is the Bohr magneton), which is the largest among all rare-earth ions, leading to the realization of a forced ferromagnetic state with the highest possible magnetization among intermetallics $R_2Fe_{14}B$ (where R is a rare-earth element).

Section 2 of the article presents some essential review information about intermetallics of type $R_2Fe_{14}B$. Section 3 describes the process of synthesizing the studied samples and their subsequent certification to control the structural-phase state. Section 4 is devoted to the conducted experiments and features of measurement techniques used in experiments with MC-1 magnetocumulative generator in ultrahigh magnetic fields. Section 5 proposes a theoretical model of the full magnetization process, formulates a methodology for calculating phase diagrams in high magnetic fields, and provides quantitative estimates of critical magnetic field values and exchange interaction constants. The section Conclusions lists the main results and draws conclusions from the conducted experimental and theoretical studies.

2. INTERMETALLICS $R_2Fe_{14}B$

Today, considerable attention is paid to studying the properties of hard magnetic materials of the R–Fe–B system and their hydrides [11], since permanent magnets based on $Nd_2Fe_{14}B$, the most important representative of compounds of the specified family, are the most effective. They are widely used in various devices and instruments and are irreplaceable in the development and advancement of several new modern technologies [12, 13].

Currently, there is active research and investigation of multicomponent compositions based on compounds $Nd_2Fe_{14}B$ through substitutions in both the neodymium sublattice and the iron sublattice. It is known that partial substitution of Fe atoms with Co atoms in compounds $R_2Fe_{14}B$ leads to an increase in the Curie temperature. The same effect is caused by the introduction of light element atoms, such as hydrogen [14, 15]. Partial replacement of Nd atoms with Dy atoms significantly increases the coercive force of hard magnetic materials [16], while Ho doping significantly improves the temperature stability of magnets [17]. Substitution of Nd atoms with Pr atoms reduces the temperature of spontaneous spin-orientation phase transition [18], and partial substitution with Eu leads to a noticeable enhancement of the rare-earth sublattice anisotropy, which also contributes to achieving a high-coercivity state [19]. Similar examples can be continued. The purpose of such substitutions and introductions is to obtain materials with a complex of predetermined functional properties and characteristics, such as Curie temperature, spin-orientation phase transition temperature, saturation magnetization, remanent magnetization, exchange constants, and magnetocrystalline anisotropy.

Through neutron diffraction studies, it was established [20] that intermetallics of the $R_2Fe_{14}B$ family possess a tetragonal structure of the space group $P4_2/mnm$ (Fig. 2). The unit cell contains 4 formula units, i.e., a total of 68 atoms. Iron atoms occupy six different crystallographic positions (4*e*, 4*c*, $8j_1$, $8j_2$, $16k_1$, $16k_2$), rare-earth atoms occupy two positions (4*f*, 4*g*), and boron atoms occupy one position (4*f*).

Under normal conditions, several representatives of the $R_2Fe_{14}B$ family and their hydrides are

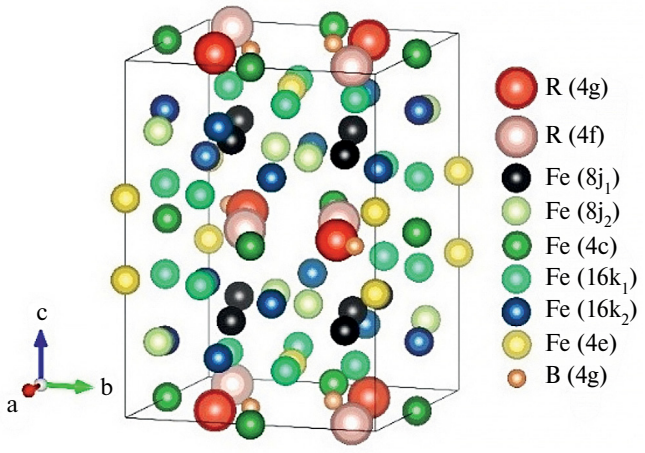

Fig. 2. Crystal structure of rare-earth intermetallics $R_2Fe_{14}B$ (schematic representation)

two-sublattice ferrimagnets, in which high and ultrahigh magnetic fields induce orientational phase transitions, accompanied by the rotation of magnetic sublattices of iron and rare-earth metal, resulting in compounds transitioning to a ferromagnetic state, i.e., completing the magnetization process in an ultrastrong magnetic field.

The values of critical transition fields, at which the sublattices begin to rotate and align parallel to the direction of the applied external magnetic field, belong to the megagauss range due to the strong exchange interaction between the rare-earth sublattice and iron sublattice (intersublattice R–Fe-exchange).

The relevance and prospects of studying compounds of type $R_2Fe_{14}B$ in high and ultrahigh external magnetic fields is determined by the fact that standard laboratory equipment, which allows measurements in magnetic fields with induction up to 30-60 T, and in exceptional cases up to 100 T, typically does not reveal all features of magnetization behavior in these compounds, especially when elements of the yttrium group (from Gd to Tm) are used as rare-earth metals, due to the large magnitude of effective fields of intersublattice exchange R-Fe interactions and significant magnitude of magnetocrystalline anisotropy constant.

Only in very high magnetic fields (often with induction of several hundred tesla) in compounds of type $R_2Fe_{14}B$ with heavy rare-earth metals is it possible to observe the process of full magnetization. As noted above, such full magnetic fields disrupt the

ferrimagnetic structure. The magnetic moments of individual sublattices (two, three, or more in multicomponent compositions) rotate relative to each other, as well as relative to the direction of the external magnetic field. The obtained experimental field dependencies of magnetization typically show changes in magnetization value (smooth or abrupt), i.e., spinorientation transitions induced by external magnetic field occur. The magnetization process is considered full (finished) when the magnetic moments of both sublattices are oriented parallel to the direction of the applied external magnetic field and forced ferromagnetic ordering is realized for the ferrimagnet.

Analysis of all features of field dependencies of magnetization in compounds of type $R_2Fe_{14}B$, observed in ultra-high magnetic fields, provides valuable information about the basic magnetic parameters of these intermetallic compounds. For compounds of type $R_2Fe_{14}B$, including multicomponent compositions, such parameters are currently not determined for many compositions with heavy rare-earth metals. Precise determination of these values has great fundamental and practical significance, including for establishing the behavior characteristics of rare-earth sublattice magnetization and its contribution's influence on the magnetic properties of these compounds.

3. METHODOLOGY FOR OBTAINING INTERMETALLIC SAMPLES AND THEIR HYDRIDES

The initial intermetallic sample $Ho_2Fe_{14}B$ was obtained by melting high-purity initial elements (R, 99.9%, Fe — 99.99%, B — 99.99%) in a "Donets-1" induction furnace in purified argon atmosphere in aluminum oxide crucibles. Due to boron's high melting temperature, the process was carried out in two stages. In the first stage, only iron and boron were preliminarily melted together, forming composition Fe_2B. In the second stage, this composition was melted together with rare-earth metal and remaining iron.

The synthesis of hydride $Ho_2Fe_{14}BH_{1.7}$ was conducted on special equipment. Fig. 3 shows the schematic diagram of the corresponding experimental setup.

For hydrogenation of samples Ho_2Fe_{14}high-purity hydrogen was used (impurity content not more than 10^{-3}% by mass), obtained by decomposition of hydride $LaNi_5H_{6+x}$ through indirect heating of reactor *3* in induction furnace *4* (Fig. 3). The process diagram, which consisted of two stages, namely, the surface activation process of samples and the hydrogenation process, is shown in Fig. 4. The amount of absorbed hydrogen was determined by calculation using the Van der Waals equation and was also verified experimentally by the combustion method. In this work, hydride $Ho_2Fe_{14}BH_{1.7}$ with relatively low hydrogen concentration was obtained.

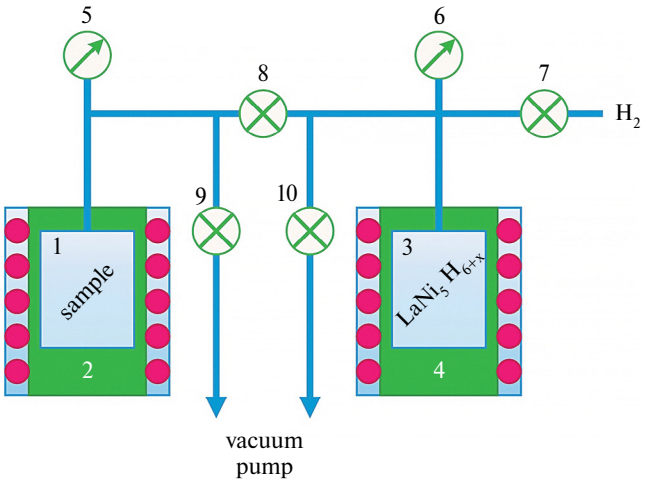

Fig. 3. Schematic diagram of the installation for hydrogenation of intermetallics R–Fe–B: *1* — hydrogenated sample, *2* and *4* — vacuum furnaces, *3* — hydride $LaNi_5H_{6+x}$, *5* and *6* — manometers, *7* – *10* – valves

Previously, it was possible to obtain a hydride $Ho_2Fe_{14}BH_{5.5}$ with the maximum possible number of hydrogen atoms per formula unit of the compound for this type of crystal structure [21, 22], and the process of its full magnetization in ultrahigh magnetic fields was studied in [23].

During hydrogenation of polycrystalline samples, the initial homogenized alloy was ground in acetone in an agate mortar to prevent oxidation of the powder during grinding. The obtained fine powder in an aluminum oxide crucible was placed (Fig. 3) in reactor *1* made of stainless steel, which was then evacuated to high vacuum using a vacuum pump. The evacuation process was carried out at room temperature and lasted 12 hours. During evacuation, the system was checked for leaks. The actual hydrogenation process was preceded by an activation process necessary for sample degassing (Fig. 4). Activation was carried out in

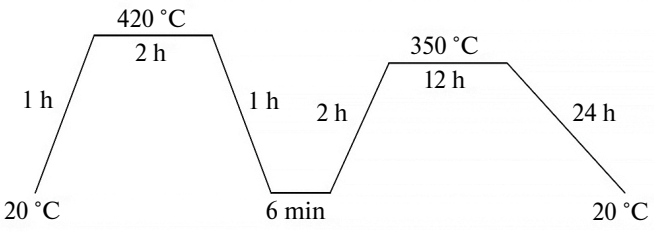

Fig. 4. Diagram of activation and hydrogenation processes in obtaining $Ho_2F_{14}BH_{1.7}$

dynamic vacuum, with indirect heating of reactor *1* containing the sample in an induction furnace *2*. The specified temperature was maintained using a temperature controller.

Experimentally, the following activation and hydrogenation sequence was chosen: first, the reactor was heated for 1 hour to temperature 420°C,which was then maintained constant until pressure stabilization in the system (approximately 2 hours), after which cooling to room temperature was carried out for 1 hour. The final pressure in the system did not exceed 0.4 mPa. The reactor was isolated from the evacuation system, and high-purity hydrogen was introduced into it. During direct hydrogenation, the sample was kept at temperature 350°C and pressure of 1 MPa for 12 hours. Finally, the entire system was slowly cooled to room temperature.

Analysis of the conducted X-ray diffraction studies [21, 22, 24] allows for monitoring the structural-phase state of synthesized compounds and determining the parameters a and c of the unit cell and its volume V both of the initial compound and its hydrides (Table 1). It was established that the incorporation of hydrogen atoms does not change the type of crystal lattice but leads to its anisotropic expansion.

4. MEASUREMENTS ON MC-1 IN ULTRAHIGH MAGNETIC FIELDS

To create magnetic fields with induction values up to 600 T, a "small" magneto-cumulative generator of MC-1 type was used [7,25]. The initial magnetic field ($B \approx 17$ T) was created in a thin-walled multilayer multi-turn solenoid by discharging a capacitor bank ($W \approx 3$ MJ). Then, the magnetic flux captured by the conducting cylinder was compressed by explosion products to a diameter of about 10 mm. The flux compression time is approximately 16 μs.

Table 1. Unit cell parameters of the intermetallic crystal $Ho_2Fe_{14}B$ and its hydrides

Compound	a, nm	c, nm	V, nm^3	$\Delta V/V$
$Ho_2Fe_{14}B$	0.8752	1.1991	0.9185	—
$Ho_2Fe_{14}BH_{1.7}$	0.8789	1.2042	0.9302	0.0128
$Ho_2Fe_{14}BH_{5.5}$	0.8873	1.2150	0.9566	0.0415

In this experiment, the main focus was on the smoothness of the magnetic field pulse and the efficiency of useful volume utilization, therefore the MC-1 generator was equipped in a single-stage version. This allowed measuring the magnetization of four samples simultaneously in one experiment. The useful volume at maximum magnetic field value was a cylinder with approximate dimensions: diameter 20 mm, length 100 mm.

The reproducibility of the magnetic field from experiment to experiment was quite high. Figures 5 and 6 show characteristic oscillograms for the inductive sensor of magnetic field derivative and the dependence of magnetic field induction on time. A schematic representation of the measuring unit is shown in Figure 7. To record the magnetic field derivative, a set of inductive sensors with different sensitivities was used. This allowed measuring the magnetic field induction with accuracy not worse than 5% throughout the entire operating range of the MC-1 generator.

To exclude diamagnetic response due to induction currents in the range with high magnetic field derivatives (from 10 to 150 T/μs), before measurements, the studied samples were ground into powder and placed in a matrix of epoxy compound. Sample texturing was not performed.

A flow-through helium cryostat was used for cooling the samples, designed considering the specific operation of the MC-1 generator. First of all, the cryostat design could not use conductive materials, which would generate large induction currents and ponderomotive forces. It also had to be inexpensive and simple to manufacture due to the impossibility of preservation during explosive experiments.

The magnetization measurement of the studied samples was carried out using a wellcompensated pair of induction coils with a decompensation degree not worse than 1%. A detailed description of

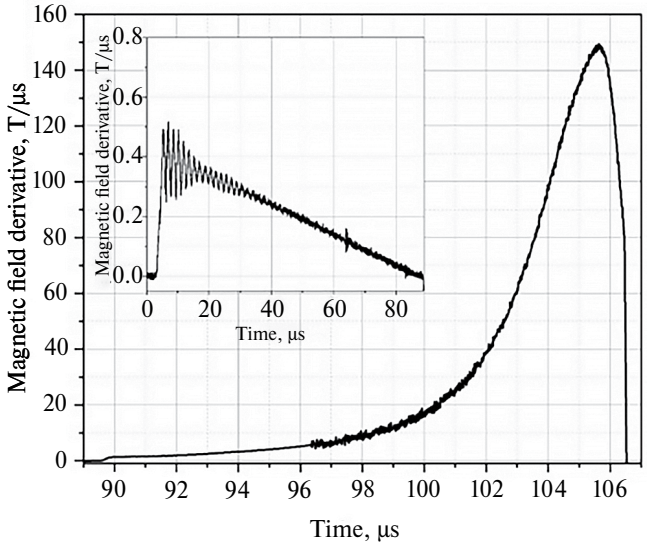

Fig. 5. Characteristic rate of magnetic field induction change for MC-1, the inset shows the same for initial field

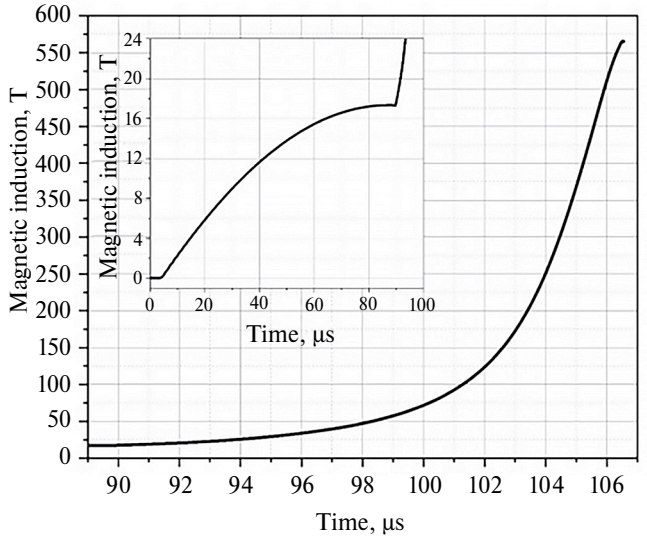

Fig. 6. Characteristic dependence of magnetic field induction on time for MC-1, the inset shows the induction of initial magnetic field

this measurement method is presented in work [26]. The coils with a diameter of $d = 3$ mm and number of turns $N = 20$ had counter-winding relative to the external magnetic field. The special winding method significantly reduces the total electrical voltage between the sensor turns, which occurs due to high rates of magnetic field change during the final stage of generator operation.

Since the measuring coils and samples are destroyed during each explosive experiment, measurements are single-time events, and it is not

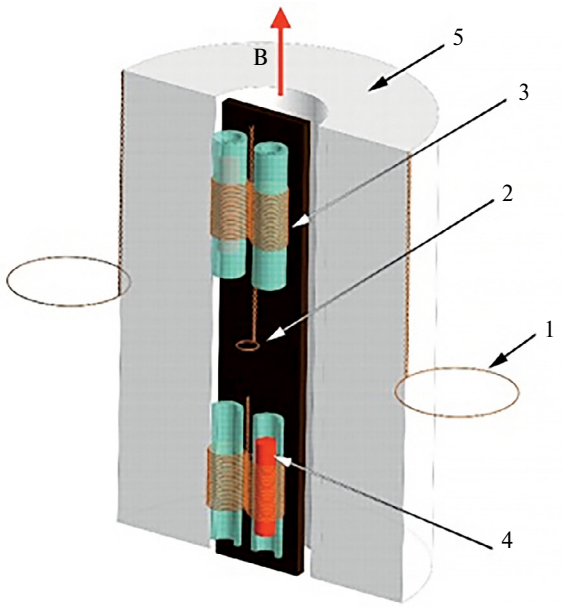

Fig. 7. Measuring unit: *1* and *2* – induction sensors for initial and enhanced field, *3* – compensation sensors, *4* – sample, *5* – cryogenic line

possible to fully compensate for the magnetic field signal. Thus, the signal from the measuring coils can be represented as

$$U(t) \propto \frac{dM}{dt} + K\frac{dH}{dt},$$

where the first term corresponds to the "useful" signal, and the second to the coil decompensation signal (K – decompensation coefficient). In the selected operating mode of the MC-generator, the decompensation is a monotonic function and does not affect measurements when studying first-order phase transitions, when magnetization changes abruptly in a small field interval, for example, during spin-flop transitions.

In this work, the main focus was on recording saturation fields, and in this case, much attention was paid to proper compensation of the coils. From several sensors, only those with minimal decompensation coefficient K were selected. Additional consideration of decompensation and zero-line shift due to addition dH/dt can be made using known magnetization measurement data for these samples in weak magnetic fields.

The results of the performed measurements – magnetization curves $Ho_2Fe_{14}B$ and its hydrides – are presented in Figures 8 and 9.

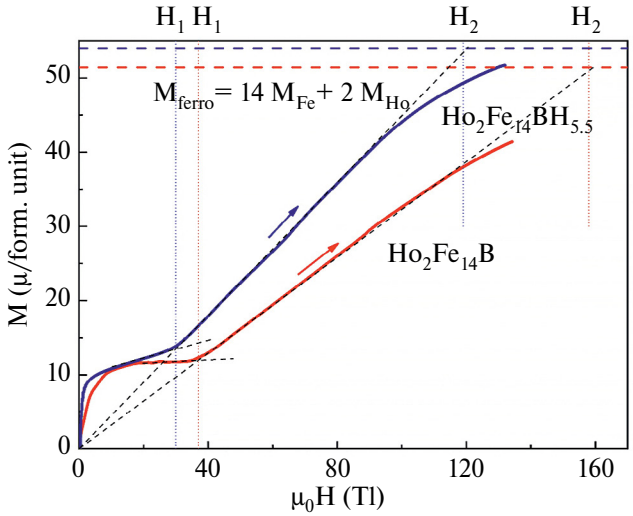

Fig. 8. Experimental magnetization curves of powder samples of rare-earth intermetallic compound $Ho_2Fe_{14}B$ and its hydride $Ho_2Fe_{14}BH_{5.5}$ with maximum hydrogen content at temperature $T = 5$ K (using measurement data performed with a single-turn solenoid [24])

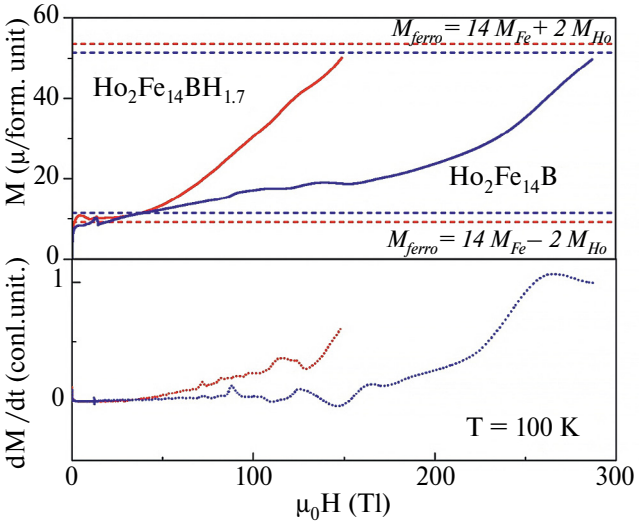

Fig. 9. (Top) experimental magnetization curves of powder samples of rare-earth intermetallic $Ho_2Fe_{14}B$ and its hydride $Ho_2Fe_{14}BH_{1.7}$ with intermediate hydrogen content; (bottom) time derivative of magnetization dM/dt. Dashed lines show magnetization values in ferrimagnetic $M_{ferri} = 14M_{Fe} - 2M_{Ho}$ and forced ferromagnetic $M_{ferro} = 14M_{Fe} + 2M_{Ho}$ phases at $T \to 0$ K

5. FULL MAGNETIZATION PROCESS AND MAGNETIC PHASE DIAGRAM

It is known [27,28] that compound $Ho_2Fe_{14}B$, as well as its hydrides under normal conditions, are two-sublattice ferrimagnets, whose magnetic structure is determined by strong exchange interaction between iron atoms and weaker exchange interaction between atoms of the iron sublattice and rare-earth sublattice. Exchange interaction between rare-earth ions is the weakest, and this interaction can be neglected.

In this case, for rare-earth ions, the exchange interaction energy with iron ions is large compared to the magnetic anisotropy energy, therefore the rare-earth sublattice can be considered as a collection of ions whose magnetic moments align along the direction of effective magnetic field $\mathbf{H}_R$, including external $\mathbf{H}$ and exchange $\mathbf{H}_{ex}$ magnetic fields:

$$\mathbf{H}_R = \mathbf{H} + \mathbf{H}_{ex} = \mathbf{H} - \lambda \mathbf{M}_{Fe}.$$

In this expression $\lambda > 0$ — is the exchange interaction constant, and $\mathbf{M}_{Fe}$ is the magnetization of the iron sublattice.

The magnetization dependence M_R of the rare-earth sublattice on the effective magnetic field H_R and temperature T, generally speaking, is determined by the spectrum of the rare-earth ion in the crystal field. However, the contribution to the crystal energy due to the interaction of the ion with an external ultrastrong magnetic field significantly exceeds the energy caused by the interaction of the ion with the crystal field, therefore, the explicit form of the dependence мости $M_R(T, H_R)$ can be approximated by the Brillouin function:

$$M_R = M_{0R} B_J \left(\frac{\mu_R H_R}{k_B T} \right).$$

Here M_{0R} is the magnetization of the rare-earth sublattice at zero temperature, J is the quantum number of the total angular momentum of the rare-earth ion.

The expression for the anisotropy energy W_A of the crystal as a whole can be represented in the single-ion approximation, where iron and rare-earth sublattices make independent contributions:

$$W_A = W_{Fe} + W_R = W_{Fe}(\theta, \varphi) + W_R(\theta', \varphi'),$$

where θ, φ, θ', φ' are angles determining the orientation of sublattice magnetizations relative to crystallographic axes. In the case of the considered uniaxial crystals, in the expression for the anisotropy energy in the first approximation, one can limit oneself to the leading term

$$W_A(\theta, \varphi) = -K_1 \sin^2 \theta, \qquad (1)$$

written in the coordinate system, where axes x and z are directed along the crystallographic a- and c-axes respectively. The anisotropy constant K_1 is positive.

The uniaxial anisotropy energy (1) reflects the existence of a preferred direction in the singlecrystal sample, along which the sublattice magnetizations align. The process of full magnetization in a single crystal is theoretically considered in work [23]. However, in the nontextured polycrystalline powder samples studied in this work, consisting of a large number of crystallites whose easy magnetization axes are randomly oriented in space, such a preferred direction is absent, which corresponds to an isotropic medium, therefore in expression (1) we should set $K_1 = 0$. This circumstance also allows us to neglect the temperature dependence of the anisotropy constant.

In addition, the anisotropy energy is relatively small compared to the exchange interaction energy [29–31]. In paper [32], it was shown that accounting for anisotropy leads to a minor revision of critical field estimates. In this work, we study the behavior of the compound in the noncollinear phase in ultra-high fields, where exchange energy is dominant, and the anisotropy contribution is corrective.

It is also necessary to point out the following circumstance: in reality, the observed dependence of the anisotropy constant for the compound $Ho_2Fe_{14}B$ is non-monotonic [33], it is maximum at a temperature of about 150 K and rapidly decreases with temperature reduction practically to zero. This feature is associated with the presence of a spin orientation transition [33, 34] occurring at temperature $T = 57.6$ K, when the sublattice magnetizations become noncollinear (the angle $\Delta\theta$ between the sample magnetization and c-axis reaches its maximum value 23° at $T \to 0$ K). Quantitatively, this effect is explained by the action of the crystal field on holmium ions [35].

In an ultra-high magnetic field, the crystal field contribution is no longer dominant, therefore, in the first approximation, one can limit oneself to the framework of the considered two-sublattice ferrimagnet model. This is supported by our obtained data on the full magnetization process: already in fields of about 20 T, ferrimagnetic saturation is achieved (Figs. 8 and 9), while the relevant fields under consideration are significantly higher.

To analyze the behavior of sublattice magnetizations in an external magnetic field, one can use the thermodynamic approach described in the monograph [36]. For this, the free energy of the compound (per unit volume), taking into account all the above remarks, can be represented as

$$F = -M_{\mathrm{Fe}} H \cos\theta - \int_0^{H_{\mathrm{R}}} M_{\mathrm{R}}\, dH_{\mathrm{R}} - K_1 \sin^2\theta. \quad (2)$$

In this work, we will consider the case of an external magnetic field directed along the initial direction of ferrimagnetic saturation, where the effective magnetic field value

$$H_{\mathrm{R}} = \sqrt{H_{ex}^2 + H^2 - 2H_{ex} H \cos\theta}.$$

The equilibrium values of angle θ can be determined using the necessary condition for the minimum of free energy (2),

$$\frac{\partial F}{\partial \theta} = M_{\mathrm{Fe}} H \sin\theta - M_{\mathrm{R}} \frac{dH_{\mathrm{R}}}{d\theta} - K_1 \sin 2\theta = 0. \quad (3)$$

In zero external field, this equation has obvious solutions $\theta = 0$ and $\theta = \pi$, satisfying the sufficient minimum condition $\partial^2 F/\partial\theta^2 > 0$.

However, when an external magnetic field is applied within a certain range of its induction at specific temperatures, solutions $\theta \neq 0$ and $\theta \neq \pi$, exist, corresponding to a noncollinear phase, i.e., a phase in which the sublattice magnetizations deviate from the direction of the applied magnetic field. Let's establish the conditions for the realization of such a phase.

From equation (3), it directly follows that the noncollinear phase is described by the relation

$$M_{\mathrm{Fe}} H - \frac{\lambda M_{\mathrm{R}} H}{H_{\mathrm{R}}} B_J\left(\frac{\mu_{\mathrm{R}} H_{\mathrm{R}}}{k_B T}\right) + 2K_1 \cos\theta = 0, \quad (4)$$

where the boundaries of its existence region in the magnetic field can be obtained by setting $\cos\theta = 1$ in this relation. Equation (4) has solutions only under the condition that the temperature T does not exceed a certain limit value T_{max}, which can be estimated using the formula

$$T_{max} = \frac{J+1}{3J} \frac{M_{\mathrm{R}}}{M_{\mathrm{Fe}}} \frac{\mu_{\mathrm{R}} H_{ex}}{k_B}.$$

If the temperature is less than the specified maximum, then the existence of a noncollinear phase is possible if the external magnetic field induction is greater than H_1, but less than H_2, called the first (lower) and second (upper) critical induction values, respectively. These values can be determined analytically from equation (4).

Measurement data [24, 32] of full magnetization curves in ultra-high magnetic fields, however, allow direct determination of the first critical field value and approximation of the second one. Figures 8 and 9 show experimentally obtained magnetization curves of the considered intermetallic compound and its hydrides at temperatures of 5 K and 100 K in external magnetic fields up to 300 T.

Based on experimental data, it is possible to calculate the constants of the studied material and its hydrides with sufficient accuracy using equation (4). In Figure 8, thin dashed lines reflect the theoretical course of the magnetization curve in all three realized phases: horizontal sections correspond to ferri- and ferromagnetic phases, the inclined section corresponds to the noncollinear phase. The inflection points (in reality – sharp changes in the curve slopes) correspond to critical fields H_1 and H_2.

Fig. 9 was used to determine the values of critical fields for the hydride with intermediate hydrogen content. The same figure shows magnetization curve measurements in fields up to 300 T at 100 K, but these data are less reliable for numerical estimates since significant measurement errors accumulate in high fields. This is the reason for the change in gradient dM/dH in the noncollinear phase $H_1 < H < H_2$ as the magnetic field induction increases, which contradicts the theoretical model.

Numerical estimates of critical fields H_1 and H_2, recalculated to zero temperature, and parameters of the studied compounds are given in Table 2. For the non-hydrided composition $Ho_2Fe_{14}B$ the exchange field value equals 98 T. Note that hydriding of the intermetallic compound significantly affects its physical characteristics. Thus, the effective exchange field value notably decreases, and with it the critical temperature of the noncollinear phase realization.

For comparison, let us also present data on estimates of the effective exchange field value from various sources.

Table 2. Material constants of ferrimagnets $Ho_2Fe_{14}BH_x$ (H_1 and H_2 at $T \to 0$ K)

x	H_1, T	H_2, T	H_{ex}, T	T_{max}, K
0	37	159	98	157
1.7	35	147	91	142
5.5	30	120	75	111

In work [33], the intersublattice exchange constant was estimated from temperature dependence measurements of single crystal samples' magnetization. The authors found that the exchange interaction energy between iron ions and rare-earth ions equals $1.44 \cdot 10^{-22}$ J, which leads to an estimate of $H_{ex} \approx 15$ T.

In work [37], magnetization curves of single crystals along different crystallographic directions are described based on the crystal field Hamiltonian taking into account exchange interaction. The authors provide an averaged estimate for the exchange field $2\mu_B H_{ex}/k_B = 310$ K, i.e. $H_{ex} = 231$ T (257 T for Ho^{3+} ions in f-positions, and in g-positions – 205 T).

Finally, analysis of magnetization curves in high magnetic fields (up to 18 T), conducted in work [34], gives the closest value to our obtained exchange field: 136 T.

We see that there is contradictory information in the literature about the magnitude of the effective exchange field, therefore the question of its determination remains relevant. In the works cited above, this value is considered as a fitting parameter, therefore, based only on measurements in relatively weak fields, it is impossible to obtain a reliable estimate for it. However, through studies of the full magnetization curve, it is possible to perform, in essence, a direct measurement of the exchange constant with sufficient accuracy. Nevertheless, we believe that further measurements on single crystal samples with the construction of a more accurate (although significantly more cumbersome theory of the full magnetization process) are necessary, however, this is beyond the scope of the tasks solved in this work.

Quantitatively, the temperature dependencies of the critical fields H_1 and H_2 in the entire temperature range $0 < T < T_{max}$ can be obtained by numerical solution of equation (4). The graphs of these dependencies are shown in Fig. 10.

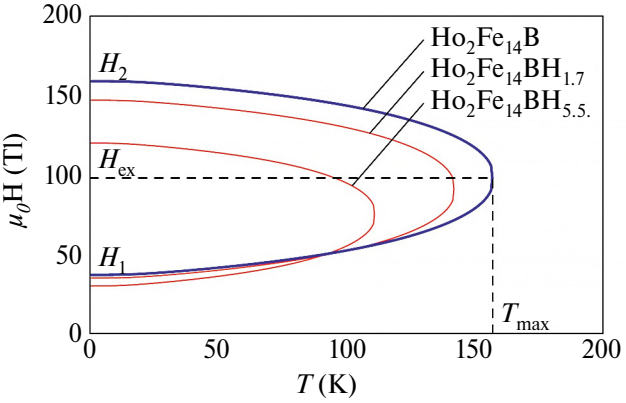

Fig. 10. Temperature dependencies of critical fields H_1 and H_2 for $Ho_2Fe_{14}B$ (blue curve) and its hydrides (red curves): at $H < H_1$ — ferrimagnetic phase, at $H > H_2$ — ferromagnetic phase, at $H_1 < H < H_2$ — noncollinear phase

In fact, these graphs represent phase H–T-diagrams of the studied compounds in ultrastrong magnetic fields. If the external magnetic field induction does not exceed the lower critical value, the intermetallic compound is in a ferrimagnetic state, where the magnetizations of the rare-earth and iron sublattices are antiparallel. When the lower critical field induction is reached, a phase transition occurs, a noncollinear phase is realized, in which the sublattice magnetizations deviate from the ferrimagnetic saturation axis, undergoing reorientation towards ferromagnetic ordering, which is realized when the field induction exceeds the upper critical value. The described process is a process of complete magnetization. Note that as the temperature increases, the lower critical field increases while the upper one decreases, and they become equal to each other at $T \to T_{max}$.

The behavior of free energy during the transition between collinear and non-collinear phases indicates the type of phase transition. Indeed, near the transition point, the angle θ is small, therefore, expanding the free energy in a series, we obtain

$$F = a(T,H)\theta^2 + b(T,H)\theta^4 + \ldots,$$

where the function $a(T,H)$ becomes zero at the boundary between phases, and the function $b(T,H)$ is positive at this boundary. Such form of free energy is characteristic of second-order phase transitions [38]. The angle value θ can be considered as an order parameter. At $\theta = 0$ (collinear phase) the ferrimagnet is invariant with respect to arbitrary rotations around the magnetic field induction vector. At $\theta \neq 0$ (non-collinear phase, where sublattice rotation occurs) this invariance disappears. The transition occurs with symmetry reduction in accordance with Landau's theory of second-order phase transitions.

6. CONCLUSIONS

The main results and conclusions of this work can be formulated as follows: magnetization measurements of rare-earth intermetallic ferrimagnet $Ho_2Fe_{14}B$ and its hydrides were performed in ultrahigh magnetic fields of the megagauss range, a model of complete magnetization process was constructed, allowing to estimate the values of critical fields inducing transitions from ferrimagnetic phase to non-collinear (H_1) and from non-collinear to ferromagnetic (H_2). Based on the extracted data, magnetic phase diagrams of these compounds were quantitatively calculated, and estimates of intersublattice exchange interaction constants were provided.

The conducted measurements allowed experimental observation of the field-induced phase transition from the initial ferrimagnetic state to the non-collinear state. To complete the full magnetization process and observe both compounds in the forced ferromagnetic state, magnetic fields with induction belonging to the megagauss range are required.

Although the theoretical model of the complete magnetization process developed in this work is quite simple, it proves sufficient to describe the main features of the magnetization curve in ultrahigh magnetic fields and to estimate the process characteristics and parameters of the studied compounds. With minimal modifications, the presented model can be applied to study the magnetic properties of rare-earth magnets of various compound classes in high and ultrahigh magnetic fields.

FUNDING

This study was carried out within the framework of the scientific program of the National Center for Physics and Mathematics (NCPM), project "Research in High and Ultrahigh Magnetic Fields" (code "NCPM-7-2325"). The work of N.V.K. was supported by the Ministry of Science and Higher

Education of the Russian Federation (contract 075-03-2023-106, project FSMG-2021-0005). The work of D.I.P. was supported by the RUDN University Strategic Academic Leadership Program. The work of G.A.P. was carried out within the framework of the state assignment for fundamental research, topic code FSEG-2023-0016.

REFERENCES

1. V. L. Ginzburg, UFN **174**, 1240 (2004).
2. V. M. Kaspi and A. M. Beloborodov, Ann. Rev. Astron. Astrophys. **55**, 261 (2017).
3. L.-D. Kong, S. Zhang, S.-N. Zhang et al., Astrophys. J. Lett. **933**, L3 (2022).
4. A. D. Sakharov, UFN 88, 725 (1966).
5. A. I. Bykov, M. I. Dolotenko, N. P. Kolokolchikov et al., Physica B: Cond. Mat. **294-295**, 574 (2001).
6. D. Nakamura, A. Ikeda, H. Sawabe et al., Rev. Sci. Instr. **89**, 095106 (2018).
7. M. I. Dolotenko, *MC-1 Magnetocumulative Generators of Ultrahigh Magnetic Fields*, RFNC-VNIIEF, Sarov (2015).
8. G. V. Boriskov, A. I. Bykov, M. I. Dolotenko et al., UFN **181**, 441 (2011).
9. A. K. Zvezdin, I. A. Lubashevsky, R. Z. Levitin et al., UFN **168**, 1141 (1998).
10. A. K. Zvezdin, V. V. Kostyuchenko, V. V. Platonov et al., UFN **172**, 1303 (2002).
11. I. S. Tereshina, N. Yu. Pankratov, A. Yu. Karpenkov et al., J. Appl. Phys. 130, 220902 (2021).
12. O. Gutfleisch, M. A. Willard, E. Brück et al., Adv. Mater. **23**, 821 (2011).
13. J. M. D. Coey, Engineering **6**, 119 (2020).
14. G. Delette, J. Magn. Magn. Mater. **577**, 170768 (2023).
15. L. A. Ivanov, T. Kaminskaya, I. Tereshina et al., Sol. St. Phenomena **312**, 235 (2020).
16. W. F. Li, H. Sepehri-Amin, T. Ohkubo et al., Acta Materialia **59**, 3061 (2011).
17. I. S. Tereshina, I. A. Pelevin, E. A. Tereshina et al., J. Alloys Compounds **681**, 555 (2016).
18. I. S. Tereshina, G. A. Politova, T. P. Kaminskaya et al., Scientific and Technical Bulletin of SPbSPU, Physical and Mathematical Sciences **15**, 34 (2022).
19. J. Chaboy, N. Plugaru, J. Bartolomé et al., Phys. Rev. B **67**, 014415 (2003).
20. J. F. Herbst, J. J. Croat, and W. B. Yelon, J. Appl. Phys. **57**, 4086 (1985).
21. I. S. Tereshina, A. P. Pyatakov, E. A. Tereshina-Chitrova et al., AIP Adv. **8**, 125223 (2018).
22. I. S. Tereshina, L. A. Ivanov, E. A. TereshinaChitrova et al., Intermetallics **112**, 106546 (2019).
23. N. V. Kostyuchenko, D. I. Plokhov, V. V. Dorofeev et al., Engineering Physics, Issue **5**, 12 (2024).
24. N. V. Kostyuchenko, I. S. Tereshina, E. A. Tereshina-Chitrova et al., Phys. Rev. Mater. 5, 074404 (2021).
25. A. I. Bykov, E. A. Bychkova, S. V. Galanova et al., in *Proceedings of XXVII International Symposium on Nanophysics and Nanoelectronics* (Nizhny Novgorod, 2023), IAP RAS, Nizhny Novgorod (2023), p. 311.
26. Yu. B. Kudasov, *Electrophysical Measurements*, Fizmatlit, Moscow (2010).
27. J. F. Herbst, Rev. Mod. Phys. **63**, 819 (1991).
28. I. S. Tereshina, Doctoral Dissertation in Physics and Mathematics, MSU, Moscow (2003).
29. V. I. Silantyev, A. I. Popov, R. Z. Levitin, A. K. Zvezdin, JETP **78**, 640 (1980).
30. G. A. Babushkin, A. K. Zvezdin, R. Z. Levitin et al., JETP **80**, 1952 (1981).
31. H. B. Callen, *Thermodynamics and an Introduction to Thermostatistics*, Wiley (1991).
32. N. V. Kostyuchenko, I. S. Tereshina, A. V. Andreev et al., IEEE Trans. Magn. **57**, 2101105 (2021).
33. S. Hirosawa, Y. Matsuura, H. Yamamoto et al., J. Appl. Phys. **59**, 873 (1986).
34. G. Givord, H. S. Li, J.M. Cadogan et al., J. Appl. Phys. 63, 3713 (1988).
35. H. Hiroyoshi, R. Kato, M. Yamada et al., Sol. St. Commun. **62**, 475 (1987).
36. K. P. Belov, A. K. Zvezdin, A. M. Kadomtseva et al., *Orientation Transitions in Rare-Earth Magnetics*, Nauka, Moscow (1979).
37. T. S. Zhao and J. I. Lee, J. Appl. Phys. **75**, 3008 (1994).
38. L. D. Landau, E. M. Lifshitz, *Statistical Physics*, Fizmatlit, Moscow (2021).